Research Square

Preprints are preliminary reports that have not undergone peer review.
They should not be considered conclusive, used to inform clinical practice,
or referenced by the media as validated information.

Induction of teleomorphic structures in the golden flower fungus, Eurotium cristatum, using dried or water-immersed Fuzhuan brick tea

Chul Jong Yoon
Research Institute of Electron Microscopy
Ki Woo Kim
kiwoo@knu.ac.kr
Kyungpook National University https://orcid.org/0000-0002-7010-0336

Research Article

Keywords: Ascocarp, Aspergillus, Fermentation, Xerophile

Posted Date: November 25th, 2026

DOI: https://doi.org/10.21203/rs.3.rs-11691054/v1

License: This work is licensed under a Creative Commons Attribution 4.0 International License.
Read Full License

Research

Induction of teleomorphic structures in the golden flower fungus, *Eurotium cristatum*, using dried or water-immersed Fuzhuan brick tea

Chul Jong Yoon[1] and Ki Woo Kim[2,3*]

[1]*Research Institute of Electron Microscopy, Gimpo 10066, Republic of Korea*

[2]*Department of Forest Ecology and Protection, Kyungpook National University, Sangju 37224, Republic of Korea*

[3]*Tree Diagnostic Center, Kyungpook National University, Sangju 37224, Republic of Korea*

Running Head: Golden flower fungus on Fuzhuan brick tea

[*]*Corresponding author*: kiwoo@knu.ac.kr

Abstract

The external and internal structures of the "golden flower fungus", *Eurotium cristatum*, were investigated via light and electron microscopy. Fuzhuan brick tea was selected as a post-fermented dark tea substrate for fungal growth. The tea was sectioned into segments to serve as either dried or water-immersed substrates. Stereomicroscopy revealed the teleomorph of *E. cristatum*, characterized by mycelia and yellow cleistothecia on both dried and water-immersed Fuzhuan brick tea. Scanning electron microscopy revealed ruptured globose cleistothecia and ascospores exhibiting a convex, rough surface with a distinct furrow in the equatorial region. Additionally, low-voltage imaging disclosed ascus-like membranes enveloping these clustered ascospores. Transmission electron microscopy revealed the ultrastructure of *E. cristatum* hyphae containing vacuoles that harbored autophagic bodies. These findings provide a practical baseline for the microscopic analysis of *E. cristatum* and for elucidating the metabolic pathways involved in enhancing the yield of "golden flowers" in post-fermented tea.

Keywords Ascocarp, *Aspergillus*, Fermentation, Xerophile

Introduction

Tea is the most popular non-alcoholic beverage consumed worldwide, second only to water (Piyasena et al. 2026). All types of tea are primarily produced from the tea plant, *Camellia sinensis*, with the major varieties being *C. sinensis* var. *sinensis* and *C. sinensis* var. *assamica* (Harbowy and Balentine, 1997). In China, tea is conventionally classified into six categories based on the processing techniques: (i) green tea (unfermented), (ii) white tea (slightly fermented), (iii) yellow tea (partly fermented), (iv) Oolong tea (semi-fermented), (v) black tea (fully fermented), and (vi) dark tea (post-fermented) (Ning et al. 2017). Among these, post-fermented dark tea has gained considerable attention due to its anti-obesity effects, which lower serum total cholesterol, triglycerides, and low-density lipoprotein cholesterol through the inhibition of lipid absorption and biosynthesis (Zhang et al. 2013).

Fuzhuan brick tea (FBT), one of the most representative types of dark tea, is primarily produced in the Hunan, Sichuan, and Yunnan provinces of China, where it is compressed into a brick form from the older and coarser leaves of *C. sinensis* (Du et al. 2022; Zheng et al. 2015). The traditional manufacturing process of FBT consists of ten major steps: (1) first rolling, (2) primary pile fermentation, (3) second rolling, (4) drying, (5) blending, (6) steam piling, (7) secondary pile fermentation, (8) compact shaping, (9) fungus fermentation (golden flowering), and (10) packaging and storage (Chen et al. 2023).

Microbial community analysis of FBT has revealed that "golden flowers" comprise various fungal genera, such as *Aspergillus, Eurotium*, *Debaryomyces*, *Pestalotiopsis*, *Rhizomucor*, and *Verticillium*, some of which produce golden cleistothecia on the surface of the tea leaves (Li et al. 2026; Zhang and Zhang, 2024). The ascomycete *Eurotium cristatum*, the teleomorph of *Aspergillus* section *Aspergillus*, dominates the fungal community in FBT (Qi and Sun 1990; Chen et al. 2023). Consequently, this fungus is widely referred to as the "golden flower fungus" (GFF). Polyhydroxy anthraquinones are known to impart yellow, orange, or brown pigmentations to the fungus (Deng et al. 2023). The GFF is typically found inside FBT lumps. Consequently, optimizing its proliferation conditions is crucial to maximize its commercial potential.

Following amendments to the botanical code, species of the genus *Eurotium* were transferred to the genus *Aspergillus* with respective nomenclatural updates for each species (Hubka et al. 2013). Thus, *E. cristatum* was renamed as *A. cristatus* (syn. *A. cristatellus*), although both names remain in use. The genus *Eurotium* is morphologically characterized by golden cleistothecia, lenticular ascospores, uniseriate conidial heads in shades of green or blue, and hyphae encrusted with yellow, orange, or red pigments (Deng et al. 2023). Micromorphology of *A. cristatus* was revealed by light and scanning electron microscopy (SEM) on solid media, such as Czapek yeast autolysate agar with 20% (w/v) sucrose and Harrold's agar with 60% (w/v) sucrose (Hu et al. 2024; Hubka et al. 2013; Xu et al. 2011). Surface features of the *E. cristatum* spore polysaccharide were imaged using atomic force

microscopy as well as SEM (Zhang et al. 2025).

However, limited information is available regarding the micromorphology and ultrastructure and of the GFF on FBT and the water surface using SEM and transmission electron microscopy (TEM). Furthermore, visual documentation of ascocarp development on the tea plant surface remains scarce. The present study reports the micromorphology and ultrastructure of GFF via stereomicroscopy, SEM, and TEM, establishing a baseline for its practical application in the tea industry.

Methods

Specimens for the golden flower fungus

The GFF was prepared in two forms for microscopy: (i) dried specimens isolated from FBT, and (ii) water-immersed specimens obtained from stationary cultures grown on the water surface.

(i) Dried specimens

Commercial FBT (~1 kg) were produced in Hunan, China, and obtained from a tea supplier (Gaoma Erxi, Seoul, Korea). The FBT lump exhibited a dark brown to black coloration

interspersed with yellow stalks (Fig. 1). The lump was sectioned into segments (~5 cm × 10 cm) and air-dried at room temperature (25–30 °C) for microscopy.

(ii) Water-immersed specimens

To evaluate the potential for GFF biomass proliferation in liquid culture, FBT segments were floated on distilled water in a plastic container. They were then incubated under stationary conditions at room temperature for at least 3 days.

Stereomicroscopy

Mycelia and cleistothecia at various developmental stages, including initial and mature forms, were collected from the dried specimens. Additionally, the fungal materials grown on the water surface were harvested. These specimens were observed using a stereomicroscope (EZ4 HD; Leica Microsystems, Heerbrugg, Switzerland).

Scanning electron microscopy

Two types of protocols were employed: (i) direct mounting for dried specimens and (ii) a conventional preparation for water-immersed specimens. For dried specimens, smaller

123 dried FBT segments (~1 cm × 1 cm) were excised from the dried FBT and mounted on
124 aluminum stubs using double-sided copper tape (Yoon and Kim 2026). The mounted
125 segments were coated with gold using an ion coater (IB-3; Eiko, Tokyo, Japan). The
126 specimens were then observed using a scanning electron microscope (S-3000N; Hitachi,
127 Tokyo, Japan) operated at 5~10 kV.

128 For water-immersed specimens, the mycelia and cleistothecia were harvested and
129 processed as previously reported (Kim, 2021; Yoon et al. 2025). Briefly, the fungal
130 materials were pre-fixed in 2.5% glutaraldehyde and 1.5% paraformaldehyde in 0.05 M
131 sodium cacodylate buffer (pH 7.4), followed by post-fixation with 2% osmium tetroxide.
132 They were then dehydrated in a graded ethanol series and dried using a critical point dryer
133 (EM CPD 300; Leica Microsystems). The specimens were mounted, coated, and observed
134 as described above for the dried specimens.

135

136 ***Transmission electron microscopy***

137

138 The mycelia were collected from the liquid culture and processed according to the method
139 described by Yoon et al. 2025). Briefly, the specimens were pre-and post-fixed as described
140 for SEM observation. They were then dehydrated in a graded ethanol series, infiltrated with
141 propylene oxide, and embedded in an Epon 812 resin mixture. After polymerization,
142 ultrathin sections were obtained using an ultramicrotome (MT6000; Sorvall, USA) and

mounted on copper grids. The sections were stained with 2% uranyl acetate followed by Reynolds' lead citrate and then observed using a transmission electron microscope (JEM-1400; JEOL, Tokyo, Japan) at 80 kV.

Results

Stereomicroscopy revealed the teleomorph of GFF, characterized by mycelia and cleistothecia on a dried segment of the FBT lump (Fig. 2a). These fungal structures formed on both the leaves and stalks of the tea plant. The cleistothecia were globose, yellow, and ~70 μm in diameter (Fig. 2b). GFF also proliferated on tea segments floated on distilled water at 28 °C for 3 days (Fig. 2c). Similar cleistothecia were observed on the plastic container under identical conditions (Fig. 2d). However, the GFF culture was frequently co-cultured with a black fungal species (Fig. 2e). Magnified views revealed globose, black conidial heads that likely belonged to an *Aspergillus* species (Fig. 2f).

Scanning electron microscopy revealed distinct mycelia and cleistothecia of GFF on a dried segment of the FBT lump (Fig. 3a). Magnified views showed fungal hyphae growing over the cleistothecia (Fig. 3b). Some cleistothecia were partially ruptured, exposing the inner ascospores (Figs. 3c–g). The ascospores, ~5 μm in diameter, exhibited a convex, rough surface with a distinct furrow in the equatorial region (Fig. 3h).

Ruptured cleistothecia released ascospores that had been displaced from their

internal surfaces (Fig. 4a). Magnified views demonstrated clustered ascospores arranged in a globose configuration (Fig. 4b). Notably, low-voltage (6–7 kV) imaging revealed ascus-like membranes enveloping these clustered ascospores (Fig. 4c).

The fungal teleomorphic structures, including cleistothecia, in the liquid culture were similar to those observed on dried tea segments (Fig. 5a). However, fungal contaminants with tiny conidia were readily distinguishable from GFF structures. An *Aspergillus* species was clearly visible, characterized by a globose conidial head and numerous tiny conidia (Fig. 5b). Magnified views revealed pumpkin-like conidia (~3 μm in diameter) featuring a rough, wrinkled surface and uneven ridges (Fig. 5c).

Transmission electron microscopy frequently revealed the ultrastructure of GFF hyphae (Fig. 6a). These hyphae contained nuclei and lipid globules in the cytoplasm, alongside vacuoles harboring autophagic bodies. Similar vacuoles were frequently observed in other hyphae as well (Fig. 6b). Magnified views disclosed the presence of one or several vesicles and electron-dense structures within the vacuoles (Fig. 6c).

Fungal hyphae contained Woronin bodies near the septa within the cytoplasm (Fig. 7a). These bodies exhibited nearly homogeneous matrices and were bounded by a single membrane. Vacuole fusion was also noted within the hyphae (Fig. 7b). Magnified views revealed a vacuole fusing with an adjacent vacuole (Figs. 7c, d).

Discussion

This study provided the micromorphology and ultrastructure of the GFF through the combined use of light and electron microscopy. While previous studies have primarily focused on the fungal structures on solid media, such as agar medium, this study demonstrates them on FBT and liquid culture. The teleomorphic structures, including cleistothecia, ascospores, and asci, were observed on dried tea segments. These micromorphological characteristics were overall consistent with those of GFF reported in previous studies in terms of color, size, and shape (Abliz et al. 2001; Hubka et al. 2013). These results strongly suggest that the yellow fungus is highly likely to be *E. cristatum*. In addition, ultrastructural analysis of the hyphae revealed autophagic processes, which are known to be associated with fungal starvation induced by dried tea substrates and nutrient-deficient liquid culture (Nitsche et al. 2013). To the best of our knowledge, this is the first report to provide detailed micromorphological and ultrastructural descriptions of GFF.

While the teleomorphic structures were frequently found within the crevices of the dried leaves, they were not observed on the leaf surfaces directly exposed to the air. Consequently, isolating or harvesting large quantities of the GFF remains challenging, as the yellow cleistothecia predominantly form within these crevices. To address this limitation, we attempted to cultivate the GFF under liquid culture conditions to induce the formation of yellow cleistothecia. Our findings demonstrate that liquid culture is highly

effective for the formation of both mycelia and cleistothecia of the GFF. Further studies are required to optimize culture conditions to maximize the yield of these teleomorphic structures, especially the visually desirable yellow cleistothecia for enhancing GFF abundance in FBT.

The occurrence of vacuoles containing autophagic bodies in the cytoplasm indicates that the GFF underwent autophagy. When filamentous fungi encounter nutrient starvation in nature, they undergo cellular degeneration, autolysis, and even cell death (Pollack et al. 2009). Autophagy is a process involving the degradation of degenerated organelles for cellular adaptation to adverse environments (Glick et al. 2010; Jung et al. 2019). It is characterized by the occurrence of vesicles within vacuoles in plants and fungi (Nakatogawa, 2020). These cellular events are strikingly similar to those observed in the vacuoles of the GFF in this study. Consistently, the fungal vacuoles were found to harbor sequestered cytoplasmic materials. The vacuole fusions observed in the hyphae are suggested to represent an autophagic pathway for vacuolar degradation. All species of *Eurotium* are xerophilic fungi that are widely distributed in natural and harsh environments, particularly in high-salt, high-sugar, and low-moisture habitats (Deng et al. 2023; Visage et al. 2017). Taken together, these results suggest that E. cristatum undergoes autophagy under these growth conditions, a process likely linked to its xerophilic nature for surviving in nutrient-deficient environments.

It is well established that ascospores develop within asci in Ascomycota. *Eurotium*

223 species are known to possess clustered eight ascospores within a globose ascus in light
224 micrographs (Abliz et al. 2001; Yoon et al. 2009; Xu et al. 2010). However, asci have not
225 been clearly observed in the scanning electron micrographs of *Eurotium* species to date,
226 including *E. chevalieri* and *E. rubrum* isolated from wheat (Clarke and Griffiths, 1970), *E.*
227 *cristatum* isolated from soil (Abliz et al. 2001), *E. halophilicum* isolated from library books
228 (Micheluz et al. 2015), and *E. rubrum* isolated from Meju (Yun et al. 2009). A recent work
229 demonstrated the presence of naked asci in *Taphrina wiesneri*, a fungal pathogen of
230 witches' broom in cherry trees, using SEM at 5 kV (Ahn et al. 2026). Although asci were
231 not observed in micrographs taken at 10 kV, they became visible at 6–7 kV in this study.
232 This observation aligns with the findings of Joy and Joy (1996), who reported that a 200
233 Å-thick carbon film supported by a copper grid was invisible at 20 kV but became visible at
234 1 kV. This contrast occurs because the electron interaction volume at lower voltages is
235 entirely contained within the specimen's thickness. Taken together, these observations
236 indicate that fungal asci may go undetected under high-voltage SEM imaging in spite of
237 their actual presence, potentially leading to misleading conclusions and misinterpretations
238 of fungal structures. Therefore, low-voltage SEM imaging should be considered as a critical
239 approach for revealing the characteristics of asci.
240

241 # Conclusions

242

Teleomorphic structures of GFF, including cleistothecia and ascospores, were induced using dried or water-immersed FBT. Light and electron microscopy visualized these structures, showing yellow cleistothecia, ascus-bound clustered ascospores, and autophagic processes in the hyphae. These findings provide a practical baseline to characterize GFF and elucidate the metabolic pathways underlying the functional attributes of post-fermented tea.

List of Abbreviations

Fuzhuan brick tea: FBT

Golden flower fungus: GFF

Scanning electron microscopy: SEM

Transmission electron microscopy: TEM

Declarations

Availability of data and materials

Data and materials will be made available upon request.

Competing interests

The authors declare no competing interests relevant to this article.

Ki Woo Kim is an editor-in-chief of *Applied Microscopy*. This status has no bearing on

263 editorial consideration.

264

265 Funding

266 Not applicable.

267

268 Authors' contributions

269 All authors collaborated on all aspects of the research and manuscript writing in this study.

270

271 Acknowledgements

272 Not applicable.

273

274 Author's information

275 Not applicable.

276

277 References

278

279 Abliz, P., Horie, Y., Hui, Y., Nishimura, K., and Li, R. 2001. New and interesting species of

280 *Eurotium* from Chinese soil. Mycoscience 42, 289–294.

281 Ahn, H., Ahn, E. J., Park, J., Seo, D., and Kim, K. W. 2026. Micromorphology of naked asci
282 and yeast cells of *Taphrina wiesneri* on *Prunus* × *yedoensis* leaves. Plant Pathology 75,
283 e70

284 Chen, G., Peng, Y., Xie, M., Xu, W., Chen, C., Zeng, X., and Liu, Z. 2023. A critical review
285 of Fuzhuan brick tea: processing, chemical constituents, health benefits and potential
286 risk. Crit. Rev. Food Sci. Nutr. 63, 5447–5464.

287 Clarke, J. H. and Griffiths, D. A. 1970. Ascospores of some common species of *Eurotium*
288 (*Aspergillus*) as shown by scanning electron microscopy. Trans. Br. mycol. Soc. 55,
289 117–122.

290 Deng, J., Li, Y., Yuan, Y., Yin, F., Chao, J., Huang, J., Liu, Z., Wang, K., and Zhu, M. 2023.
291 Secondary metabolites from the genus *Eurotium* and their biological activities. Foods
292 12, 4452.

293 Du, Y., Yang, W., Yang, C., and Yang, X. 2022. A comprehensive review on microbiome,
294 aromas and flavors, chemical composition, nutrition and future prospects of Fuzhuan
295 brick tea. Trends Food Sci. Technol. 119, 452–466.

296 Glick, D., Barth, S., Macleod, K. F. 2010. Autophagy: cellular and molecular mechanisms. J.
297 Pathol. 221, 3–12.

298 Harbowy, M. E. and Balentine, D. A. 1997. Tea chemistry. Crit. Rev. Plant Sci.
299 16:415–480.

300 Hu, Z., Liu, S., Zhou, X., Liu, Z., Li, T., Yu, S., Zhang, X., and Xu, Z. 2024. Morphological
301 variation and expressed sequence tags-simple sequence repeats-based genetic diversity
302 of *Aspergillus cristatus* in Chinese dark tea. Front. Microbiol. 15, 1390030.

303 Hubka, V., Kolařík, M., Kubátová, A., and Peterson, S. W. 2013. Taxonomic revision of
304 *Eurotium* and transfer of species to *Aspergillus*. Mycologia 105, 912–937.

305 Joy, D. C. and Joy, C. 1996. Low voltage scanning electron microscopy. Micron 27,
306 247–263.

307 Jung, M., Choi, H., and Mun, J. 2019. The autophagy research in electron microscopy. Appl.
308 Microsc. 49, 11.

309 Kim, K. W. 2021. Morphology and surface characteristics of the anamorphic stage of
310 powdery mildew *Erysiphe australiana* on crape myrtle leaves. Micron 143, 103013.

311 Li, S., Wang, Q., Du, X., He, B., and Zhang, J. 2026. Fermentation with *Aspergillus*
312 *cristatus* changed the volatile compounds and metabolites of Fu-brick Tea: Insights
313 from aroma profiling and widely targeted metabolomics. Fermantation 12, 339.

314 QiMicheluz, A., Manente, S., Tigini, V., Prigione, V., Pinzari, F., Ravagnan, G., and Varese,
315 G. C. 2015. The extreme environment of a library: Xerophilic fungi inhabiting indoor
316 niches. Int. Biodeterior. Biodegrad. 99, 1–7.

317 Nakatogawa, H. 2020. Mechanisms governing autophagosome biogenesis. Nat. Rev. Mol.
318 Cell Biol. 21, 439–458.

319 Ning, J., Sun, J., Li, S., Sheng, M., and Zhang, Z. 2017. Classification of five Chinese tea
320 categories with different fermentation degrees using visible and near-infrared
321 hyperspectral imaging. Int. J. Food Prop. 20, S1515–S1522.

322 Nitsche, B. M., Burggraaf-van Welzen, A. M., Lamers, G., Meyer, V., and Ram, A. F. J.
323 2013. Autophagy promotes survival in aging submerged cultures of the filamentous
324 fungus *Aspergillus niger*. Appl. Microbiol. Biotechnol. 97, 8205–8218.

325 Piyasena, K. G. N. P., Napagoda, M. T., Kalinga, J., and Jayasinghe, L. 2026. Health
326 benefits of different types of tea: a review. Food Nutr. Health 3, 11.

327 Pollack, J. K., Harris S. D., and Marten, M. R. 2009. Autophagy in filamentous fungi.
328 Fungal Genet. Biol. 46, 1–8.

329 Qi, Z. T. and Sun, Z. M. 1990. Identification of predominant species in brick tea. Acta
330 Mycol. Sin. 9, 176–179.

331 Visage, C. M., Yilmaz, N., Renaud, J. B., Sumarah, M. W., Hubka, V., Frisvad, J. C., Chen,
332 A. J., meijer, M., and Seifert, K. A. 2017. A survey of xerophilic *Aspergillus* from
333 indoor environment, including descriptions of two new section *Aspergillus* species
334 producing eurotium-like sexual states. MycoKeys 19, 1–30.

335 Xu, A., Wang, Y., Wen, J., Liu, P., Liu, Z., and Li, Z. 2011. Fungal community associated
336 with fermentation and storage of Fuzhuan brick-tea. Int. J. Food Microbiol. 146,
337 14–22.

338 Yoon, C. J. and Kim, K. W. 2026. Fractography of white charcoal reveals past fungal
339 infection and embolism in the secondary xylem via SEM. Appl. Microsc. 56, 5.

340 Yoon, C. J., Chi, J. G., and Kim, K. W. 2025. Encapsulation, vacuolation and phagocytosis
341 of the opportunistic fungal pathogen *Cryptococcus* in the liver of an immunocompetent
342 host. Microscopy 74, 286–292.

343 Yun, Y. H., Hyun, M. W., Suh, D. Y., Kim, Y. M, and Kim, S. H. 2009. Identification and
344 characterization of *Eurotium rubrum* isolated from Meju in Korea. Mycobiology 37,
345 251–257.

346 Zhang, L., Cheng, M., Tian, Y., and Wang, Z. 2025. Structural characterization of *Eurotium*
347 *cristatum* spore polysaccharide and its hypoglycemic and hypolipidemic ability *in*
348 *vitro*. Inter. J. Biol. Macromol. 307, 142296.

349 Zhang, L., Zhang, Z.-Z., Zhou, Y.-B., Ling, T.-J., and Wan, X.-C. 2013. Chinese dark teas:
350 Postfermentation, chemistry and biological activities. Food Res. Int. 53, 600–607.

351 Zhang, Q. and Zhang, J. 2024. Overview of *Eurotium cristatum* and its fermentation
352 application in tea. FIM 3, 11–20.

353 Zheng, W.-J., Wan, X.-C., and Bao, G.-H. 2015. Brick dark tea: a review of the manufacture,
354 chemical constituents and bioconversion of the major chemical components during
355 fermentation. Phytochem. Rev. 14, 499–523.

356

357

Figure Captions

Fig. 1. Photograph of a Fuzhuan brick tea lump, showing a dark brown to black coloration interspersed with yellow stalks.

Fig. 2. Stereomicrographs of *Eurotium cristatum.* (**a**) Yellow cleistothecia (arrows) on a dried segment of a Fuzhuan brick tea lump. (**b**) Magnified view of yellow cleistothecia on the tea segment. (**c**) Yellow mycelia (arrows) grown on tea segments floated on distilled water at 28 °C for 3 days. (**d**) Yellow cleistothecia (arrows) grown on the plastic container under the same conditions as in (c). (**e**) *Aspergillus* species (arrows) grown under the same conditions as in (c). (**f**) Magnified view of the *Aspergillus* species (arrows) grown under the same conditions as in (c). Scale bars = 100 μm in (a–e); and 500 μm in (f).

Fig. 3. Scanning electron micrographs of *E. cristatum* on dried segments of a Fuzhuan brick tea lump. (**a**) Mycelia and cleistothecia (arrows). (**b**) Magnified view of the dashed rectangle in (a). C, cleistothecium. (**c, e**) Partially cracked cleistothecia (arrows) filled with ascospores. (**d, f**) Magnified views of the dashed rectangles in (c and e). A, ascospore. (**g**) Half-cracked cleistothecium. (**h**) Ascospore. Scale bars = 500 μm in (a); 50 μm in (b, c); 5 μm in (d, f); 20 μm in (e, g); and 2 μm in (h).

Fig. 4. Scanning electron micrographs of *E. cristatum* on dried segments of a Fuzhuan brick tea lump. (**a**) Ascospores displaced from the inner surface (arrow) of a cleistothecium. S, stoma on the tea plant leaf. (**b**) Magnified view of ascospores (arrows). Note the densely clustered ascospores in a dashed circle. (**c**) Ascospores at 5 kV. Note that some ascospores were covered with asci in a dashed circle. Scale bars = 10 μm in (a, c); and 5 μm in (b).

Fig. 5. Scanning electron micrographs of *E. cristatum* and *Aspergillus* species on segments of a Fuzhuan brick tea lump floated on distilled water at 28 °C for 3 days. (**a**) Mycelia and cleistothecia (arrows). Note the contamination with *Aspergillus* conidia in a dashed circle. (**b**) Conidiophore and conidia of an *Aspergillus* species. (**c**) *Aspergillus* conidia. Scale bars = 100 μm in (a); 20 μm in (b); and 5 μm in (c).

Fig. 6. Transmission electron micrographs of *E. cristatum* hyphae. (**a**) Overview. Note the vacuoles (arrows) containing autophagic bodies. CW, cell wall; L, lipid globule; S, septum. (**b**) Magnified view of a hypha showing vacuoles (arrows). (**c**) Magnified view of the vacuoles containing autophagic bodies. Scale bars = 2 μm in (a); 1 μm in (b); and 500 nm in (c).

Fig. 7. Transmission electron micrographs of *E. cristatum* hyphae. (**a**) Longitudinal view. M, mitochondrion; S, septum; W, Woronin body. (**b**) Transverse view. V, vacuole. (**c, d**)

398 Magnified views of the dashed rectangles in (b). Note the vacuole fusions and mitochondria

399 in the cytoplasm. Scale bars = 1 μm in (a); and 500 nm in (b–d).

Fig. 1.



Fig. 2.

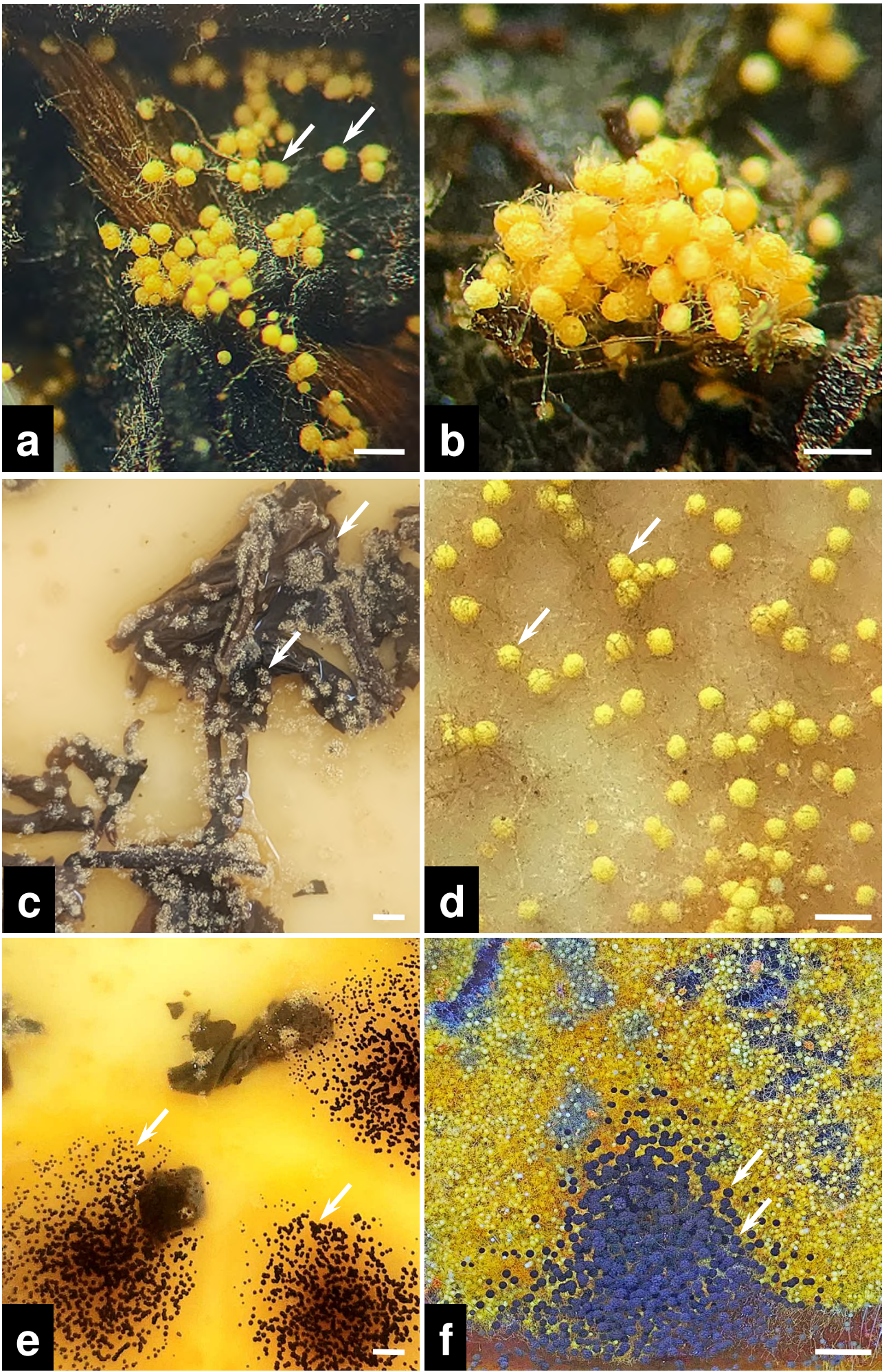

Fig. 3.

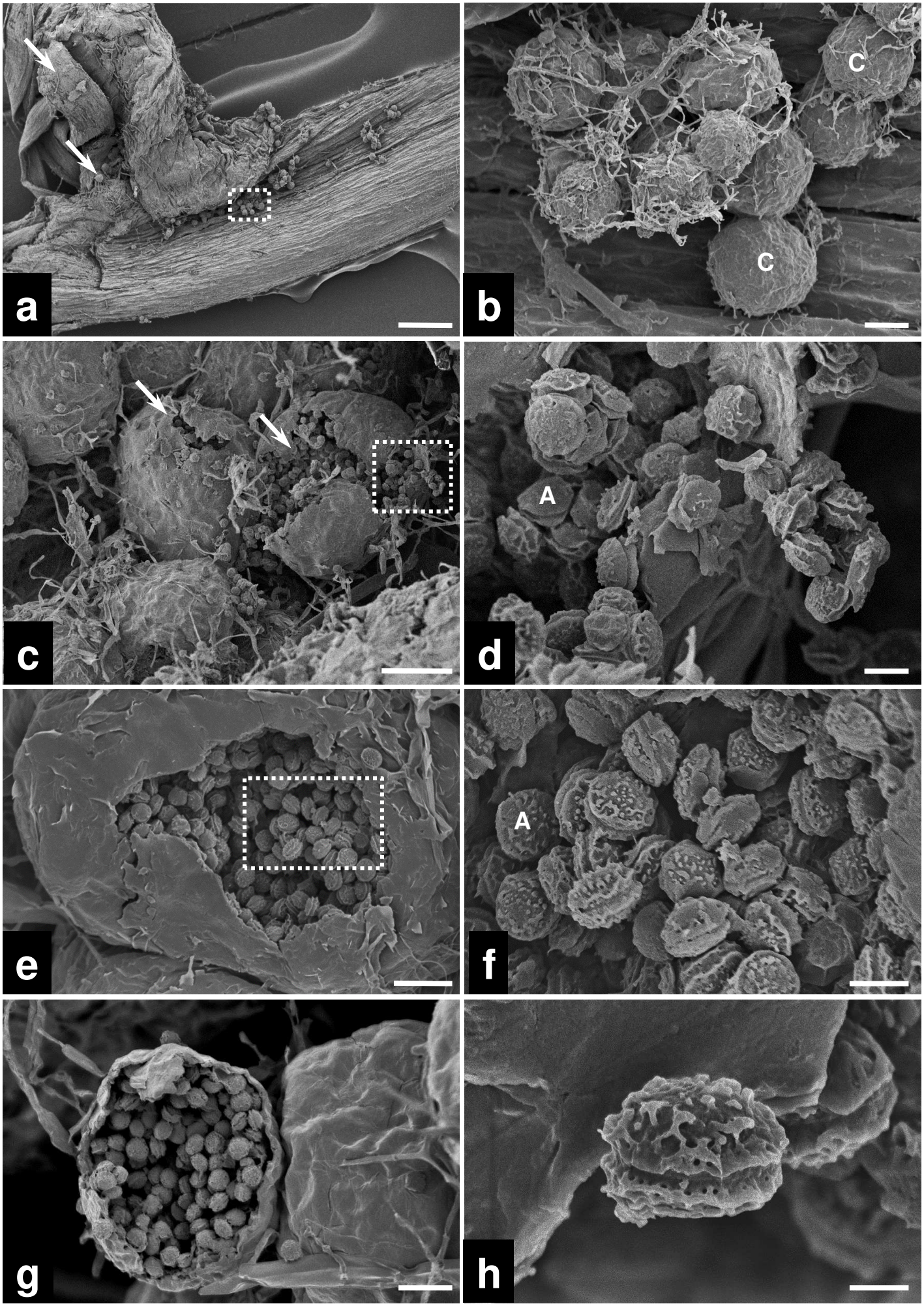

Fig. 4.

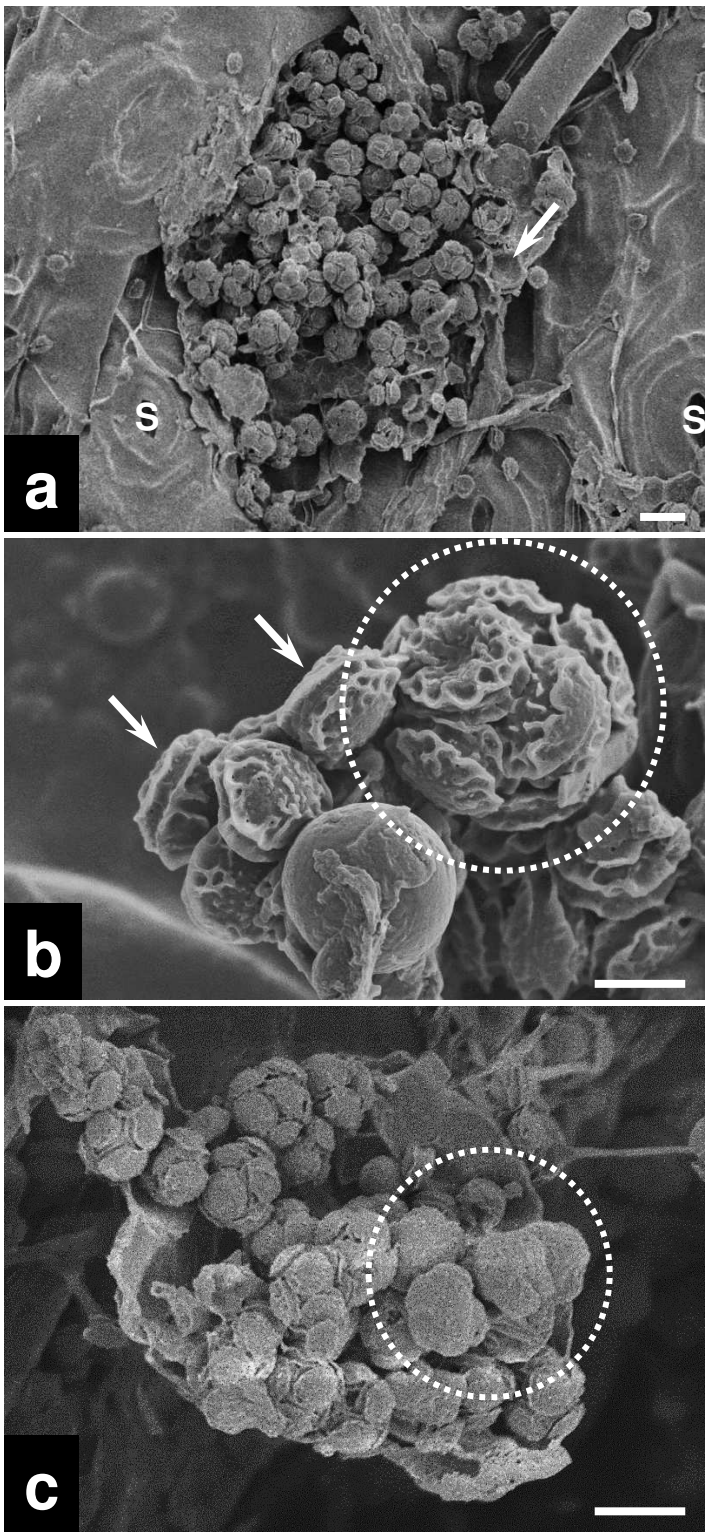

Fig. 5.

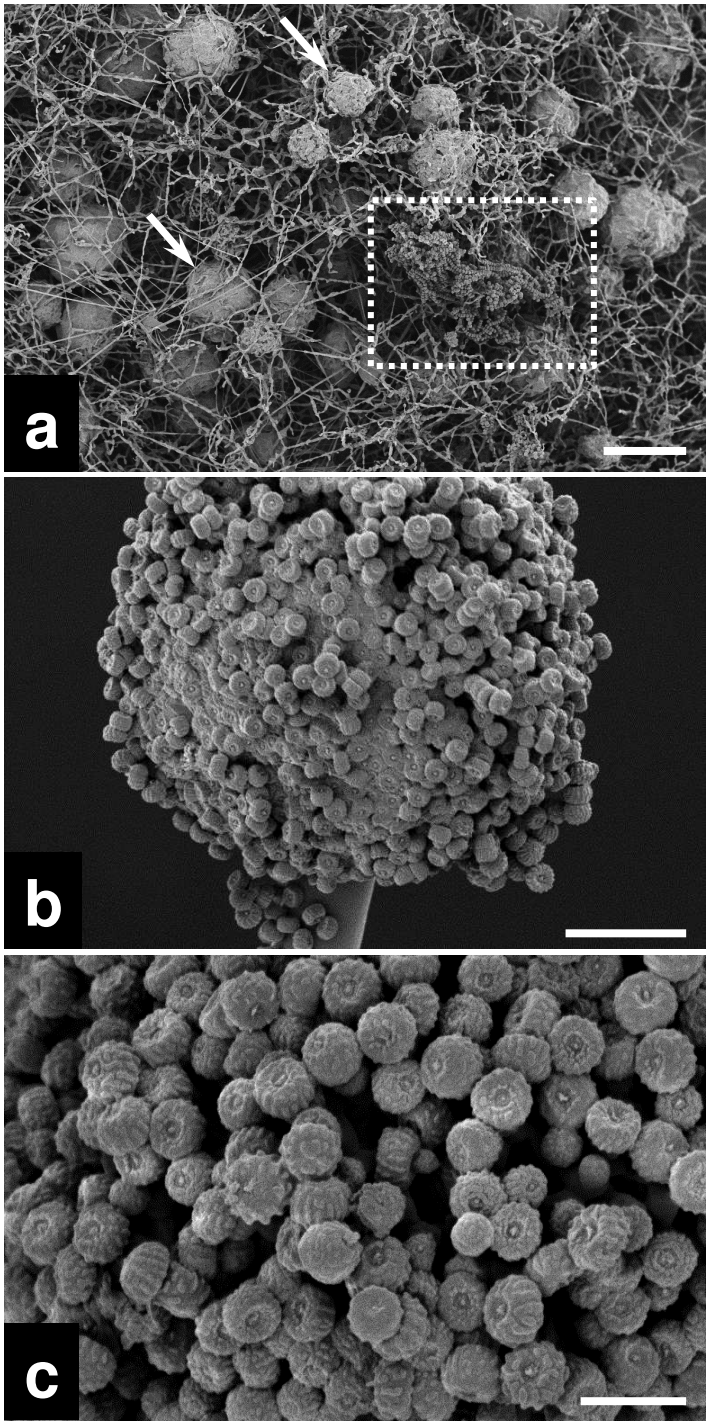

Fig. 6.

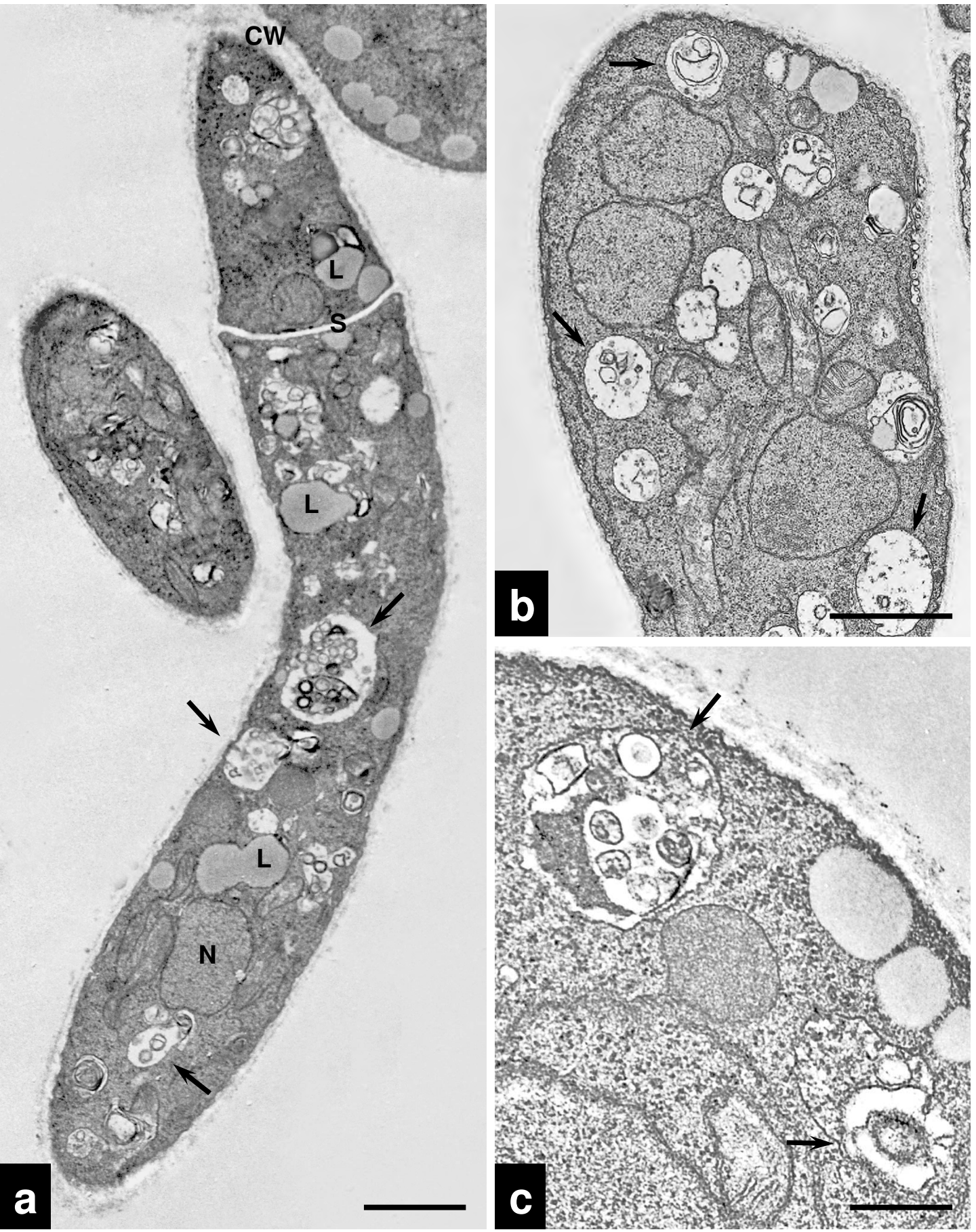

Fig. 7.

